

Revisit of Local X-ray Luminosity Function of Active Galactic Nuclei with the MAXI Extragalactic Survey

Yoshihiro UEDA,¹ Kazuo HIROI,¹ Naoki ISOBE,^{1,2} Masaaki HAYASHIDA,¹ Satoshi EGUCHI,^{1,3} Mutsumi SUGIZAKI,⁴ Nobuyuki KAWAI,⁵ Hiroshi TSUNEMI,⁶ Tatehiro MIHARA,⁴ Masaru MATSUOKA,^{4,7} Masaki ISHIKAWA,⁸ Masashi KIMURA,⁶ Hiroki KITAYAMA,⁶ Mitsuhiro KOHAMA,⁷ Takanori MATSUMURA,⁹ Mikio MORII,⁵ Yujin E. NAKAGAWA,¹⁰ Satoshi NAKAHIRA,⁴ Motoki NAKAJIMA,¹¹ Hitoshi NEGORO,¹² Motoko SERINO,⁴ Megumi SHIDATSU,¹ Tetsuya SOOTOME,⁴ Kousuke SUGIMORI,⁵ Fumitoshi SUWA,¹² Takahiro TOIZUMI,⁵ Hiroshi TOMIDA,⁷ Yohko TSUBOI,⁹ Shiro UENO,⁷ Ryuichi USUI,⁵ Takayuki YAMAMOTO,⁴ Kazutaka YAMAOKA,¹³ Kyohei YAMAZAKI,⁹ Atsumasa YOSHIDA,¹³ and the MAXI team

¹*Department of Astronomy, Kyoto University, Oiwake-cho, Sakyo-ku, Kyoto 606-8502
hiroi@kusastro.kyoto-u.ac.jp*

²*Institute of Space and Astronautical Science (ISAS), Japan Aerospace Exploration Agency (JAXA), 3-1-1 Yoshino-dai, Chuo-ku, Sagami-hara, Kanagawa 252-5210*

³*National Astronomical Observatory of Japan, 2-21-1, Osawa, Mitaka City, Tokyo 181-8588*

⁴*MAXI team, Institute of Physical and Chemical Research (RIKEN), 2-1 Hirosawa, Wako, Saitama 351-0198*

⁵*Department of Physics, Tokyo Institute of Technology, 2-12-1 Ookayama, Meguro-ku, Tokyo 152-8551*

⁶*Department of Earth and Space Science, Osaka University, 1-1 Machikaneyama, Toyonaka, Osaka 560-0043*

⁷*ISS Science Project Office, Institute of Space and Astronautical Science (ISAS), Japan Aerospace Exploration Agency (JAXA), 2-1-1 Sengen, Tsukuba, Ibaraki 305-8505*

⁸*School of Physical Science, Space and Astronautical Science, The graduate University for Advanced Studies (Sokendai), Yoshinodai 3-1-1, Chuo-ku, Sagami-hara, Kanagawa 252-5210*

⁹*Department of Physics, Chuo University, 1-13-27 Kasuga, Bunkyo-ku, Tokyo 112-8551*

¹⁰*Research Institute for Science and Engineering, Waseda University, 17 Kikui-cho, Shinjuku-ku, Tokyo 162-0044*

¹¹*School of Dentistry at Matsudo, Nihon University, 2-870-1 Sakaecho-nishi, Matsudo, Chiba 101-8308*

¹²*Department of Physics, Nihon University, 1-8-14 Kanda-Surugadai, Chiyoda-ku, Tokyo 101-8308*

¹³*Department of Physics and Mathematics, Aoyama Gakuin University, 5-10-1 Fuchinobe, Chuo-ku, Sagami-hara, Kanagawa 252-5258*

(Received ; accepted)

Abstract

We construct a new X-ray (2–10 keV) luminosity function of Compton-thin active galactic nuclei (AGNs) in the local universe, using the first MAXI/GSC source catalog surveyed in the 4–10 keV band. The sample consists of 37 non-blazar AGNs at $z = 0.002 - 0.2$, whose identification is highly ($> 97\%$) complete. We confirm the trend that the fraction of absorbed AGNs with $N_{\text{H}} > 10^{22} \text{ cm}^{-2}$ rapidly decreases against luminosity (L_{X}), from 0.73 ± 0.25 at $L_{\text{X}} = 10^{42-43.5} \text{ erg s}^{-1}$ to 0.12 ± 0.09 at $L_{\text{X}} = 10^{43.5-45.5} \text{ erg s}^{-1}$. The obtained luminosity function is well fitted with a smoothly connected double power-law model whose indices are $\gamma_1 = 0.84$ (fixed) and $\gamma_2 = 2.0 \pm 0.2$ below and above the break luminosity, $L_* = 10^{43.3 \pm 0.4} \text{ ergs s}^{-1}$, respectively. While the result of the MAXI/GSC agrees well with that of HEAO-1 at $L_{\text{X}} \gtrsim 10^{43.5} \text{ erg s}^{-1}$, it gives a larger number density at the lower luminosity range. Comparison between our luminosity function in the 2–10 keV band and that in the 14–195 keV band obtained from the Swift/BAT survey indicates that the averaged broad band spectra in the 2–200 keV band should depend on luminosity, approximated by $\Gamma \sim 1.7$ for $L_{\text{X}} \lesssim 10^{44} \text{ erg s}^{-1}$ while $\Gamma \sim 2.0$ for $L_{\text{X}} \gtrsim 10^{44} \text{ erg s}^{-1}$. This trend is confirmed by the correlation between the luminosities in the 2–10 keV and 14–195 keV bands in our sample. We argue that there is no contradiction in the luminosity functions between above and below 10 keV once this effect is taken into account.

Key words: catalogs — surveys — galaxies: active — X-rays: galaxies

1. INTRODUCTION

The tight correlation between the mass of a supermassive black hole (SMBH) in a galactic center and that of the budge found in the local universe (Magorrian et al. 1998; Ferrarese & Merritt 2000; Gebhardt et al. 2000; Marconi & Hunt 2003; Häring & Rix 2004; Hopkins et al. 2007;

Kormendy & Bender 2009; Gültekin et al. 2009) leads to an idea of the “co-evolution” of SMBHs and galaxies. Thus, understanding the growth of SMBHs is a fundamental issue to elucidate the cosmological history of the universe in the relation with the evolution of galaxies. The key objects to study this are active galactic nuclei (AGNs), the phenomena where the SMBH gains its mass by accret-

ing gas.

The most basic observational quantities to describe the cosmological evolution of AGNs is the luminosity function (LF), the number density per comoving space as a function of luminosity and redshift. To derive the AGN LF, a statistically well-defined sample (unusually, a flux limited one) with complete identification obtained by unbiased surveys is required. Hard X-ray observations at energies above a few keV provide the most efficient and complete surveys to detect the whole AGNs including obscured ones (so-called “type 2” AGNs), the major class in this population (e.g., see Gilli et al. 2007), thanks to its strong penetrating power against absorption by the surrounding material and to little contamination from stars in the host galaxy. In the past several years, combinations of hard X-ray surveys above 2 keV with different survey depths have revealed the evolution of LF of AGNs constituting the major part of the Cosmic X-ray background (CXB), which gives strong constraints on the scenario of the SMBH growth from $z = 0$ to $z \sim 5$ (e.g., Ueda et al. 2003; La Franca et al. 2005; Barger et al. 2005; Silverman et al. 2008; Ebrero et al. 2009; Yenko et al. 2009; Aird et al. 2010).

To establish the X-ray LF of AGNs in the local universe is of great importance among these efforts, since it gives the reference for any evolution models. While Ueda et al. (2003), Silverman et al. (2008), Ebrero et al. (2009), and Yenko et al. (2009) have found that the luminosity dependent density evolution (LDDE; this term was originally introduced by Miyaji et al. 2000) best describes of the X-ray AGN LF above 2 keV, Aird et al. (2010) recently suggest that the luminosity and density evolution (LADE) where the “shape” of the LF is constant over the whole redshift range gives a similarly good fit to their data. Ueda et al. (2003) employ the local AGN LF in the 2–10 keV band based on the HEAO-1 all sky survey, by using the sample consisting of 49 AGNs compiled by Shinozaki et al. (2006). Sazonov & Revnivtsev (2004) has also determined the local AGN LF in the 3–20 keV band from the RXTE/Slew survey (Revnivtsev et al. 2004), whose integrated volume emissivity corrected for incompleteness is found to be by a factor of 2 smaller than the HEAO-1 result converted into the same energy band, however.

More recently, hard X-ray surveys above 10 keV performed by the Swift and INTEGRAL satellites also determine the local AGN LF in the 14–195 keV or 15–55 keV band (Swift; Tueller et al. 2008; Burlon et al. 2011) and in the 20–40 keV or 17–60 keV band (INTEGRAL; Beckmann et al. 2006b; Sazonov et al. 2007), respectively. The advantage of these surveys is the least biases against heavily obscured AGNs, although the observed fraction of Compton thick objects with an absorption column density of $N_{\text{H}} > 10^{24} \text{ cm}^{-2}$ is found to be as small as < 5 percent in the total sample (Tueller et al. 2008; Burlon et al. 2011). It is found the shape of the AGN LF above 10 keV as determined by Swift/BAT looks significantly different from the Shinozaki et al. (2006) result if the luminosity is simply converted into the other band by assuming a typical AGN spectrum (characterized by a power law with a pho-

ton index of ≈ 1.8). The reasons of this discrepancy have not been understood yet.

Thus, it is timely to revisit the local X-ray AGN LF below 10 keV from a new survey independently, in order to check the consistency with the previous works and solve the apparent contradictions among them. The Monitor of All-sky X-ray Image (MAXI) mission on the International Space Station (Matsuoka et al. 2009), currently in orbit, provides a valuable opportunity for this. Hiroi et al. (2011) produce the first source catalog of the MAXI/Gas Slit Camera (GSC; Mihara et al. 2011; Sugizaki et al. 2011) at high galactic latitudes ($|b| > 10^\circ$), by compiling the data in the 4–10 keV band accumulated for the first 7 month since the start of its nominal operation. The catalog contains 51 AGNs detected with a significance above 7σ consisting of 39 Seyfert galaxies and 12 blazars. In this paper, we constrain the local AGN LF in the 4–10 keV band by using only non-blazar AGNs (i.e., Seyferts) in the Hiroi et al. (2011) catalog. We also determine the intrinsic distribution of absorption column density of AGNs (so-called N_{H} function) in the local universe using the same sample, and compare it with the previous results. Section 2 briefly describes the source sample and their X-ray spectral properties in terms of an absorption column density and a photon index determined from various observatories. Section 3 describes the analysis method and obtained results. We discuss the implication in Section 4. The cosmological parameters of $(H_0, \Omega_{\text{m}}, \Omega_{\Lambda}) = (70h_{70} \text{ km s}^{-1} \text{ Mpc}^{-1}, 0.3, 0.7)$ are adopted throughout the paper. The “log” symbol represents the base-10 logarithm, while “ln” the natural logarithm.

2. Sample

To investigate the local LF and N_{H} function of AGNs, we collect the 37 non-blazar AGNs from the Hiroi et al. (2011) catalog at $z = 0.002 - 0.2$ that constitute a statistically unbiased sample detected in the 4–10 keV band from an area of $34,000 \text{ deg}^2$. Here we exclude Cen A, located at $z < 0.002$, and ESO 509–066, which has double nuclei and may be contaminated by nearby sources (see Table 1 in Hiroi et al. 2011). The four “confused” sources are ignored even if they contain contribution from AGNs (like NGC 6814), which do not affect our results. As noted in Hiroi et al. (2011), the list of the X-ray brightest AGNs in the all sky has significantly changed from that of the HEAO-1 survey performed 30 years ago; among 39 MAXI/GSC detected AGNs, only 17 objects are listed in both sample by Piccinotti et al. (1982) and that used by Shinozaki et al. (2006). The flux limit of the MAXI sample corresponds to $1.5 \times 10^{-11} \text{ erg cm}^{-2} \text{ s}^{-1}$ (1.2 mCrab) in the 4–10 keV band. Figure 1 shows the $\log N - \log S$ relation (integral form) of these AGNs in the 4–10 keV band, obtained by using the area curve presented in Figure 9 of Hiroi et al. (2011).

Table 1 summarizes the AGN list, where the first to sixth columns represent the catalog source No., MAXI source name, counterparts, optical type, 4–10 keV flux, and redshift, respectively. Although it is known that us-

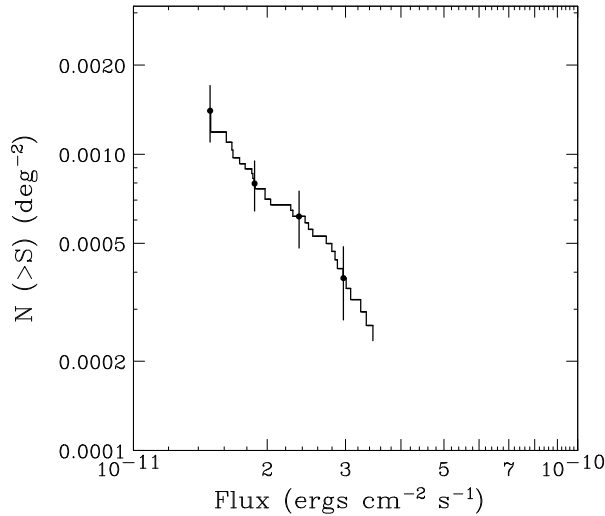


Fig. 1. $\log N - \log S$ Relation of non-blazar AGNs in the 4–10 keV band used in our analysis, determined from the first MAXI/GSC source catalog by Hiroi et al. (2011).

ing the spectroscopic redshifts to estimate the distance of very nearby objects is subject to uncertainties due to the galaxy proper motion, we adopt these values for consistency with the analysis of the Swift/BAT AGNs in Tueller et al. (2008). We confirm that even if we instead adopt redshifts corrected for the infall into the Virgo cluster by Mould et al. (2000) to calculate the luminosity of AGNs at $z < 0.01$, our results of both LF and N_H function are little affected. Here we only distinguish between two optical classes, “AGN1” (Seyfert 1.0–1.5) or “AGN2” (Seyfert 1.8–2.0), for simplicity. We can regard that this AGN sample is nearly complete (99.3%), because 142 out of the total 143 X-ray sources are identified there. The flux errors due to the statistical uncertainties are better than 14% for all the objects, and hence they are not taken into account in the following analysis.

To compare our result with the previous works easily, we construct the AGN LF in the “intrinsic” 2–10 keV luminosity corrected for the absorption (i.e., before absorption) at the source frame (hereafter represented as L_X). Since we have the count rate in the 4–10 keV band from the MAXI/GSC survey, it is necessary to convert it to L_X by using the spectral information as well as the redshift for each source. Fortunately, we are able to find results of spectral fits in the 0.2–10 (or 0.5–10) keV band in the literature for 33 (out of 37) AGNs, which were obtained from data of either *ASCA*, *XMM-Newton*, *BeppoSAX*, *Swift/XRT*, or *Suzaku*. The spectral quality is sufficiently good in most cases, and hence we neglect their errors in the following analysis. The best-fit photon index Γ , absorption column density N_H (at the source frame), and calculated luminosity from these parameters (L_X) are listed in the 7th to 9th columns of Table 1, respectively, together with the reference for the spectral parameters (10th column). In the conversion from the MAXI/GSC count rate into L_X , we consider a reflection component

from cold, optically thick matter (Magdziarz & Zdziarski 1995) with a solid angle of $\Omega = 2\pi$ as adopted in Ueda et al. (2003), although this does not affect our result of the LF. For the remaining four targets¹, we perform the same image analysis of the MAXI/GSC data in the 2–4 keV band as that in Hiroi et al. (2011) to obtain the hardness ratio between the 2–4 keV and 4–10 keV count rates. We first calculate the corresponding photon index Γ without considering any absorption; if we obtain $\Gamma < 1.9$, then we derive an absorption column density at the source redshift assuming an intrinsic power law with $\Gamma = 1.9$. The results of Γ and N_H with 1σ statistical errors estimated in this way are also listed in Table 1 for these 4 targets. Figure 2 shows the redshift (z) versus luminosity (L_X) plot for our sample. The open and filled circles correspond to those with a column density of $\log N_H < 22$ and $\log N_H < 24$, respectively. The optical type-2 AGNs are further marked with the diagonal crosses.

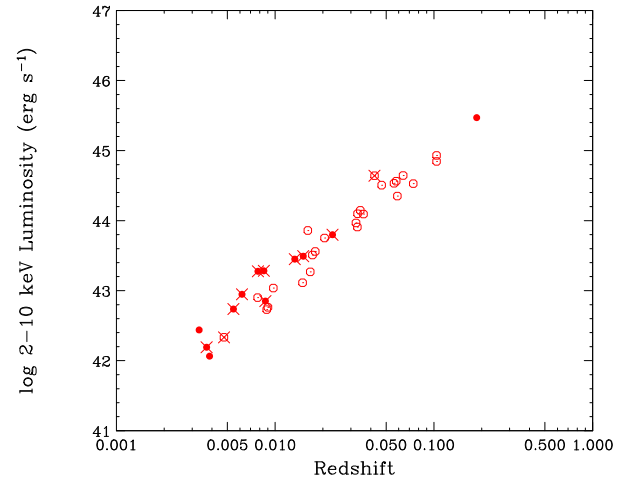


Fig. 2. Redshift versus luminosity plot of our sample. The luminosity is the intrinsic (before absorption) one in the 2–10 keV band estimated from the 4–10 keV MAXI/GSC count rate corrected for an absorption column density. The open and filled circles correspond to the X-ray unabsorbed ($\log N_H < 22$) and absorbed AGNs, respectively. Optical type 2 AGNs are marked with the diagonal crosses.

3. Analysis and Results

3.1. Analysis Method

Our goal is to determine both the N_H function and absorption-corrected 2–10 keV LF of X-ray AGNs in the local universe. The calculation follows the same procedure as presented in Ueda et al. (2003), to which we refer the reader for details. The same notation convention is adopted in this paper. The N_H function, $f(L_X, z; N_H) d\log N_H$, represents a probability of finding an AGN with an absorption column density between $\log N_H$ and $\log N_H + d\log N_H$ at a given luminosity, L_X , and redshift, z . For

¹ IRAS 05078+1626, 2MASX J09235371–3141305, 4C +18.51, 1RXS J213623.1–622400

convenience, we assign $\log N_H = 20$ for AGNs without any significant absorption, and consider only the range of $\log N_H \leq 24$, since no Compton thick AGNs are present in the current sample. It is normalized as

$$\int_{20}^{24} f(L_X, z; N_H) d\log N_H = 1. \quad (1)$$

The LF, $\Phi(L_X, z)$ in units of Mpc^{-3} , is defined so that $d\Phi(L_X, z)/d\log L_X$ gives the co-moving space density of all (Compton-thin) AGNs in a luminosity range between $\log L_X$ and $\log L_X + d\log L_X$ at a redshift of z .

From the list of N_H and L_X in our sample, the best-fit parameters are searched for by minimizing the likelihood estimator defined as

$$L = -2 \sum_i \ln \frac{N(N_{Hi}, L_{Xi}, z_i)}{\int \int \int N(N_H, L_X, z) d\log N_H d\log L_X dz}, \quad (2)$$

where the suffix i denotes each object. The term $N(N_H, L_X, z)$ represents the expected number from the survey,

$$N(N_H, L_X, z) = f(L_X, z; N_H) \times \frac{d\Phi(L_X, z)}{d\log L_X} d_A(z)^2 (1+z)^3 c \frac{d\tau}{dz}(z) A(N_H, L_X, z), \quad (3)$$

where $d_A(z)$ is the angular distance, $d\tau/dz$ the differential look back time, and $A(N_H, L_X, z)$ the survey area, given as a function of flux that is calculated from N_H , L_X , and z . The minimization process is carried out on the MINUIT software package. The 1σ error for a single parameter can be estimated from the parameter range that increases the L value by 1. The fit applied to the unbinned data here cannot estimate the normalization of the LF. Hence, we determine it so that the expected source number agrees with the observed one, and estimate its relative uncertainty only from its Poisson error ($1/\sqrt{N}$, where $N = 37$).

3.2. N_H Function

To avoid coupling between the N_H function and LF, we determine them step by step in the same way as Ueda et al. (2003), considering the small sample size. First, we constrain the N_H function by adopting the “delta-function” approximation for the LF only based on the sample list. It reduces the formula (2) to a simpler form (see equation (6) in Ueda et al. 2003) where the intrinsic N_H distribution can be evaluated directly from its observed N_H histogram by taking into account the N_H dependence of the survey area. For the four sources whose absorptions are estimated from the hardness ratios of the MAXI data and hence have non-negligible statistical errors, we take into account the uncertainties in N_H by introducing the “ N_H response matrix function” as done in Ueda et al. (2003) (see their Section 4.1).

As for the shape of the N_H function, we adopt a modified version of that used in Ueda et al. (2003). The difference from Ueda et al. (2003) is that (1) we allow such a case that the N_H function at $\log N_H < 22$ is smaller than that at $\log N_H > 22$, (2) we assign 4 discrete bins with the same width between $\log N_H = 20$ –24 for simplicity, considering the practical difficulties to determine N_H with

an accuracy better than $d\log N_H < 1$ for objects without good X-ray spectral data. We define the absorption fraction $\psi(L_X)$ as that of AGNs with $\log N_H = 22$ –24 among those with $\log N_H = 20$ –24, which is given as a function of luminosity. Its possible redshift dependence is ignored, because our sample consists of only local AGNs. The form of the N_H function is expressed differently for two $\psi(L_X)$ ranges;

$$\begin{aligned} & \text{(for } \psi(L_X) < \frac{1+\epsilon}{3+\epsilon} \text{)} \\ f(L_X, z; N_H) = & \begin{cases} 1 - \frac{2+\epsilon}{1+\epsilon} \psi(L_X) & (20 \leq \log N_H < 21) \\ \frac{1}{1+\epsilon} \psi(L_X) & (21 \leq \log N_H < 22) \\ \frac{1}{1+\epsilon} \psi(L_X) & (22 \leq \log N_H < 23) \\ \frac{1}{1+\epsilon} \psi(L_X) & (23 \leq \log N_H < 24). \end{cases} \end{aligned} \quad (4)$$

and

$$\begin{aligned} & \text{(for } \psi(L_X) \geq \frac{1+\epsilon}{3+\epsilon} \text{)} \\ f(L_X, z; N_H) = & \begin{cases} \frac{2}{3} - \frac{3+2\epsilon}{3+3\epsilon} \psi(L_X) & (20 \leq \log N_H < 21) \\ \frac{1}{3} - \frac{\epsilon}{3+3\epsilon} \psi(L_X) & (21 \leq \log N_H < 22) \\ \frac{1}{1+\epsilon} \psi(L_X) & (22 \leq \log N_H < 23) \\ \frac{1}{1+\epsilon} \psi(L_X) & (23 \leq \log N_H < 24). \end{cases} \end{aligned} \quad (5)$$

Here ϵ defines the ratio of the N_H function in $\log N_H = 23$ –24 to that in $\log N_H = 22$ –23. It is fixed at 1.3 (instead of 1.7 as adopted in Ueda et al. 2003), according to the observed N_H distribution in the Swift/BAT 9-month survey (23/18, Tueller et al. 2008), which agrees with the more recent result by Burlon et al. (2011). In the former case (equation 4), the N_H function is flat above $\log N_H = 21$, while in the latter case (equation 5), the value in $\log N_H = 21$ –22 is taken to be the mean of those at $\log N_H = 20$ –21 and $\log N_H = 22$ –23. The maximum absorption fraction is $\psi_{max} = \frac{1+\epsilon}{3+\epsilon}$, corresponding to the case of $f(N_H) = 0$ at $\log N_H = 20$ –21.

Figure 2 clearly shows that X-ray absorbed AGNs are mostly found in the lower luminosity range ($\log L_X < 44$). This confirms the trend found in many previous works (e.g., Ueda et al. 2003; Hasinger 2008) that the absorption fraction reduces with an increase of the AGN luminosity. Thus, following Ueda et al. (2003), we model the absorption fraction by a linear function of $\log L_X$ within the maximum (see above) and minimum values, which is taken to be 0.1. It is represented as

$$\psi(L_X) = \min[\psi_{max}, \max[\psi_{44} - \beta(\log L_X - 44), 0.1]], \quad (6)$$

where β and ψ_{44} are the free parameters to be determined through the likelihood fit.

Table 2 summarizes the best-fit parameters of the N_H function and their 1σ errors. Figure 3(a) plots the “intrinsic” N_H function (corrected for the observation bias) for the total sample (upper), that for low luminosities of $\log L_X < 43.5$ (middle), and that for $\log L_X > 43.5$ (lower). The dependence of the absorption fraction on the luminosity is obvious. The best-fit model of the N_H function calculated at the mean L_X value in each region is overplotted. Figure 3(b) shows the “observed” histogram of N_H for these 3 luminosity ranges, on which those predicted from the best-fit model are superposed.

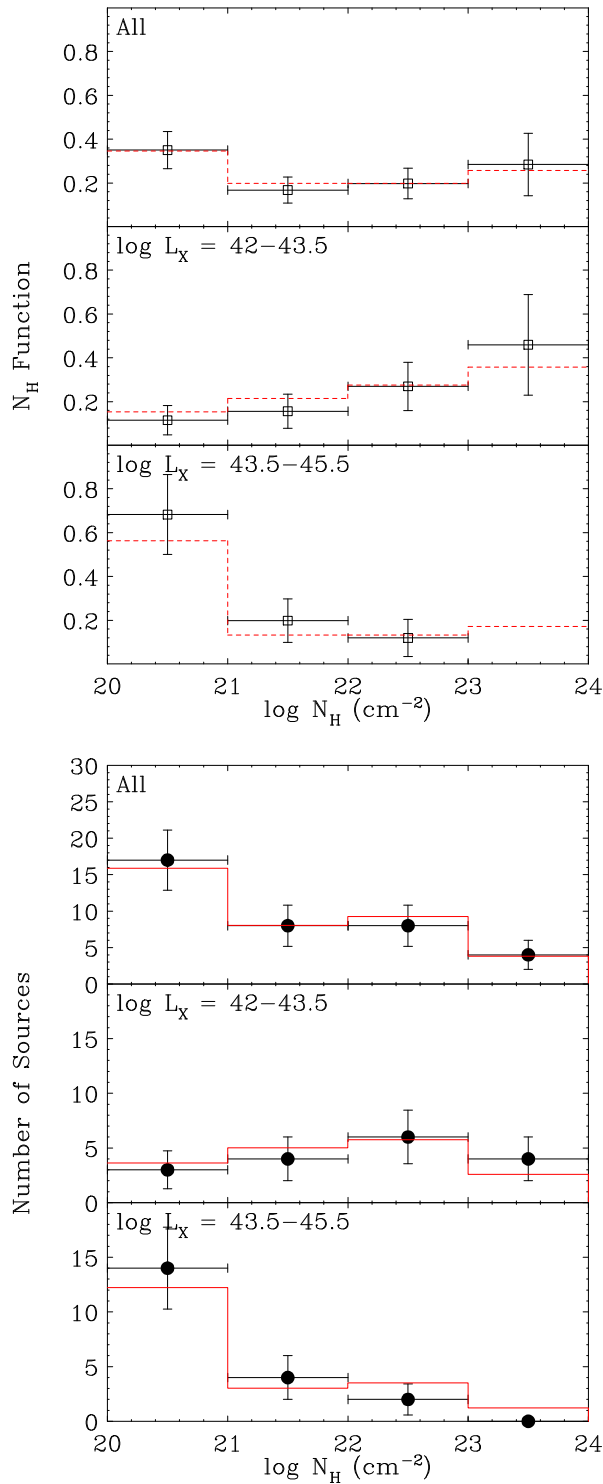


Fig. 3. (Upper) (a) Intrinsic distribution of absorption column density (N_H function). From the upper to lower panels, for the total sample, for AGNs with $\log L_X = 42-43.5$, and for AGNs with $\log L_X = 43.5-45.5$. The 1σ error is attached to the data points (open circle). The lines (red) are the best-fit N_H function calculated at the mean luminosity in each luminosity range. (Lower) (b) The observed histograms of N_H without any correction for the observational bias. The 1σ error (Poisson error) is attached to the data point (filled circle). The lines (red) show the predicted numbers in each $\log N_H$ bin calculated from the best-fit N_H function.

3.3. Luminosity Function

Using the N_H function obtained above, we finally determine the local AGN LF by maximum-likelihood fit according to the formula (2). We adopt the smoothly connected double power law model, one of the most standard descriptions for X-ray AGN LFs, given as

$$\frac{d\Phi(L_X, z=0)}{d\log L_X} = A[(L_X/L_*)^{\gamma_1} + (L_X/L_*)^{\gamma_2}]^{-1}. \quad (7)$$

To implement the effect of the cosmological evolution, we introduce the evolution factor represented by $(1+z)^{p1}$,

$$\frac{d\Phi(L_X, z)}{d\log L_X} = \frac{d\Phi(L_X, 0)}{d\log L_X} (1+z)^{p1}, \quad (8)$$

where we fix $p1 = 4.2$ based on the result obtained for the LDDE model in Ueda et al. (2003). Note that at $z < 0.2$ and $\log L_X > 42$, their LDDE model is identical with the pure density evolution model as represented above.

Due to the limited sample size, we find it difficult to constrain the three free parameters of the LF, γ_1 , γ_2 , and L_* simultaneously. Hence, we fix the power law slope in the low luminosity range at three different values, $\gamma_1 = 1.0$, $\gamma_1 = 0.84$ (the best-fit obtained from the Swift/BAT 9-month survey in Tueller et al. 2008), and $\gamma_1 = 0.62$ (the best-fit from the LADE model in Aird et al. 2010). The results of the likelihood fit for these three cases are summarized in Table 2. Figure 4 plots the best fit local LF determined from the MAXI survey for the case of $\gamma_1 = 0.84$ (black curve). The data points are calculated by the $N_{\text{data}}/N_{\text{model}}$ method (Miyaji et al. 2001), to which the 1σ statistical errors are attached according to the formula by Gehrels (1986). We find the local AGN emissivity in the 2–10 keV band integrated over the $\log L_X = 41-47$ range is $W_{2-10} = (1.37 \pm 0.23) \times 10^{39} h_{70} \text{ erg s}^{-1} \text{ Mpc}^{-3}$ for $\gamma_1 = 0.84$. This value is close to that obtained by Shinozaki et al. (2006), $W_{2-10} = (9.3 \pm 1.3) \times 10^{38} h_{70} \text{ erg s}^{-1} \text{ Mpc}^{-3}$,² but significantly larger than that by Sazonov & Revnivtsev (2004), $W_{2-10} = (4.2 \pm 0.5) \times 10^{38} h_{70} \text{ erg s}^{-1} \text{ Mpc}^{-3}$, converted from the 3–20 keV band LF by assuming a power law photon index of 2.0.

4. Discussion

We revisit the local X-ray luminosity function of non-blazar AGNs, together with the absorption distribution function, based on the first source catalog of the on-going MAXI/GSC extragalactic survey. In spite of the fact that the current MAXI/GSC source sample is smaller than those from the HEAO-1 (49 AGNs in Shinozaki et al. 2006) and RXTE (76 AGNs in Sazonov & Revnivtsev 2004) all sky surveys performed in similar energy bands, it has some advantages to firmly establish the statistical

² It is larger than that presented in Section 6.1 of Shinozaki et al. (2006), $(5.85 \pm 1.17) \times 10^{38} h_{70} \text{ erg s}^{-1} \text{ Mpc}^{-3}$. This is because while Shinozaki et al. (2006) calculated the volume emissivity using observed (i.e., absorbed) fluxes of each AGN at luminosity range of $\log L_X > 42$, we here calculate it for intrinsic (de-absorbed) luminosities by integrating the analytical expression of the LF down to $\log L_X = 41$.

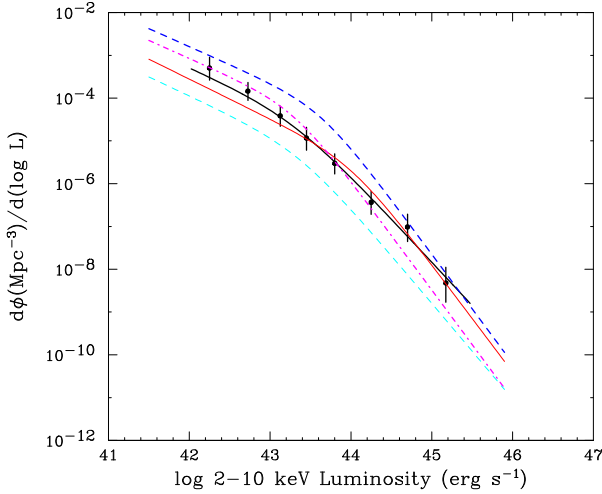


Fig. 4. Local X-ray AGN luminosity function in the 2–10 keV band. The cosmological parameters of (H_0 , Ω_m , Ω_Λ) = ($70h_{70}$ km s $^{-1}$ Mpc $^{-1}$, 0.3, 0.7) are adopted. Data points (black) are the observed values from the MAXI survey based on the “ $N_{\text{data}}/N_{\text{model}}$ ” estimator with error bars at 1σ level. The thick solid curve (black) is the best-fit model with $\gamma_1 = 0.84$ (fixed). The thin solid curve (red) and thin dashed curve (cyan) are the results from the HEAO-1 survey by Shinozaki et al. (2006) and from the RXTE slew survey by Sazonov & Revnivtsev (2004), respectively. The latter is converted from the 3–20 keV band to the 2–10 keV band for our adopted Hubble constant. The thick dashed (blue) and dot-dashed (magenta) curves are the luminosity functions derived from the Swift/BAT 9 month survey (Tueller et al. 2008) converted from the 14–195 keV band to 2–10 keV band by assuming a power law photon index of 2.0 and 1.7, respectively.

properties of AGNs below 10 keV in the following points.

(1) The sample is highly complete (99.3% = 142/143, or 97% = 37/38 in the worst case). (2) Since we have adopted a relatively conservative threshold in the source selection in our catalog (7σ), our sample is less subject to the flux uncertainties in the faintest end ($< 14\%$) and is considered to be free from Eddington’s bias as verified in $\log N - \log S$ relation (Figure 1). This could actually be a problem in the sample in Shinozaki et al. (2006), who had to correct for such biases by simulation (see their Appendix). (3) The AGN fluxes are determined from the data collected from many scans (15 times per day), and hence can be regarded as the long-term averaged flux, less affected by short term variability than those obtained from a few snap-shot observations. (4) The energy band of 4–10 keV band is more suitable for detecting obscured AGNs (except for Compton thick ones), thus reducing the observation biases for the N_H function determination. It is expected that the MAXI/GSC 4–10 keV sample has intermediate characteristics between the surveys in softer X-rays than 4 keV, and hard X-ray surveys in above 10 keV.

In fact, we find that the “observed” fraction of absorbed AGNs with $\log N_H > 22$, 32% (=12/37), is higher than the HEAO-1 (20%=10/49) and RXTE (22%=17/76) results, while it is lower than that obtained from the Swift/BAT

survey above 15 keV, 49% (=42/86; Tueller et al. 2008). We obtain the intrinsic N_H distribution by correcting for the observational biases that AGNs with heavier absorptions are harder to be detected due to the reduction of the count rates. The overall shape combined from both low and high luminosity samples (Figure 3) is well consistent with the N_H distribution obtained from the Swift/BAT survey, which show an almost flat distribution above $\log N_H > 21$ with a weak peak in the $\log N_H = 20$ –21 bin (Tueller et al. 2008). We also confirm the strong dependence of the absorption fraction on the X-ray luminosity. We obtain the best-fit formula to describe this relation slightly different from that in Ueda et al. (2003), who included much fainter AGN samples in the analysis. The slope of the absorption fraction with respect to $\log L_X$ is steep ($\beta = 0.23 \pm 0.02$ instead of $\beta = 0.10$ in Ueda et al. 2003), and reaches a higher maximum value ($\psi = 0.82$ instead of $\psi = 0.57$) at low luminosities. Such sharp (even sharper) change of the absorption fraction against the luminosity around $\log L_X \approx 43.5$ is also found in the Swift/BAT sample (Tueller et al. 2008; Burlon et al. 2011). The statistical uncertainty is quite large at present, however. It is of great importance to investigate redshift evolutions of the N_H function and the relation between the absorption fraction and luminosity by using much larger samples, which shall be left for future work.

To compare with the past results obtained from surveys in similar energy bands, we overlay the best-fit LFs obtained by Shinozaki et al. (2006) and Sazonov & Revnivtsev (2004) with the thin solid (red) and thin dashed (cyan) curves, respectively, in Figure 4. The RXTE LF is converted from the 3–20 keV band into the 2–10 keV band by assuming a photon index of 1.7 in our adopted cosmological parameters ($H_0 = 70$ km s $^{-1}$ Mpc $^{-1}$ instead of $H_0 = 75$ km s $^{-1}$ Mpc $^{-1}$ in Sazonov & Revnivtsev 2004). The systematic uncertainties due to the choice of photon index are small in this case (18% in the luminosity within a range of 1.7–2.0). Here, the normalization of the LF is corrected for the maximum factor of incompleteness (1/0.7), assuming that the unidentified targets are all AGNs whose luminosity and redshift distribution is the same as those of the identified sample. As already reported by Sazonov & Revnivtsev (2004), the RXTE result lies significantly lower than the HEAO-1 results by a factor of ~ 2 . The origin for this discrepancy is unclear, but we do not pursue it further in this paper.

As clearly seen in Figure 4, our MAXI LF is much closer to the HEAO-1 LF than the RXTE LF. In particular, it is in good agreement with the HEAO-1 result at high luminosity range above $\log L_X = 43.5$. However, the MAXI LF gives a larger number density at lower luminosities by a factor of ~ 2 –3. By assuming a similar slope of the LF in the low luminosity range ($\gamma_1 = 0.84$ –1.0), the MAXI LF favors a smaller break luminosity, $\log L_*$, 42.9–43.9, than the best-fit HEAO-1 value ($\log L_* = 44.0 \pm 0.4$), though within the statistical errors. The discrepancy can be partially explained if the absorption fraction at these low luminosity range is underestimated than the reality in the previous work. In fact, according to the best-fit

N_H function, the absorption fraction at $\log L_X = 42.5$ is estimated to be $\psi = 0.72 \pm 0.04$ in our work, while it is $\psi = 0.65$ in Ueda et al. (2003). Due to the coupling with the N_H function in constraining the LF parameters through the maximum likelihood fit (see equation (2)), the estimated LF for all AGNs with $\log N_H = 20\text{--}24$ would become smaller if we assume a lower absorption fraction in the N_H function, because it is hard to detect objects with large column densities of $\log N_H > 23$ in the 2–10 keV band survey, and its space density can be only constrained by the extrapolation from the lower column-density range.

Comparison of our AGN LF in the 2–10 keV band with the hard X-ray (> 10 keV) LF determined with the Swift/BAT and INTEGRAL surveys provides insights on the broad band properties of local AGNs. Since the fraction of Compton-thick AGNs in those hard X-ray surveys are negligibly small, we can directly compare them with our result obtained for Compton-thin AGNs. In Figure 4, we also plot the best-fit form of the LF by Tueller et al. (2008) by converting the luminosity from 14–195 keV to 2–10 keV. In this case, the assumption of the spectrum strongly affects the result. We adopt two photon index, $\Gamma = 1.7$ (thick dot-dashed, magenta) and $\Gamma = 2.0$ (thick dashed, blue). Obviously, the shape of the LF is not the same between these bands if a single spectrum index is assumed for all AGNs. At low luminosity range of $\log L_X \lesssim 44$, the normalizations of the two LFs become consistent with each other for $\Gamma \sim 1.7$, while at higher luminosities, the conversion with $\Gamma \sim 2.0$ gives a better agreement.

This result indicates that the averaged shape of broad band X-ray spectra of these AGNs depends on the luminosity, in the sense that more luminous AGNs show a steeper slope in the 2–200 keV range on average. To confirm this picture, we make the correlation plot of luminosity between the 2–10 keV and 14–195 keV bands using our MAXI sample (Figure 5). Here the hard X-ray luminosities are taken from the Swift/BAT 22-month catalog except for two AGNs that are not detected there; 2MASX J18470283–7831494 for which we refer to the Swift/BAT 58-month catalog, and 4C +18.51, which is not yet detected by the 58 month data and has only a flux upper limit of 1.1×10^{-11} erg cm $^{-2}$ s $^{-1}$ in the 14–195 keV band. We plot two lines corresponding to a power law photon index of $\Gamma = 1.7$ (solid, magenta) and $\Gamma = 2.0$ (dashed, blue). The trend that the AGNs with lower luminosities have flatter slope is indeed seen.

We have shown that since the dependence of the averaged X-ray broad band spectra on luminosity makes the direct comparison of LFs constructed in different energy bands (below and above 10 keV) not straightforward, its apparent difference in the LF shape is not “contradiction”. This effect must be taken into account when one constructs a LF in a uniform way by compiling results of X-ray surveys performed in different energy bands. There are two explanations for the reasons of the luminosity dependence of the 2–200 keV spectra. Recent studies of nearby AGNs have suggested that the intrinsic power law components of Seyfert 1 are steeper than those of Seyfert 2 (e.g., Malizia et al. 2003; Beckmann et al. 2006a; Tueller

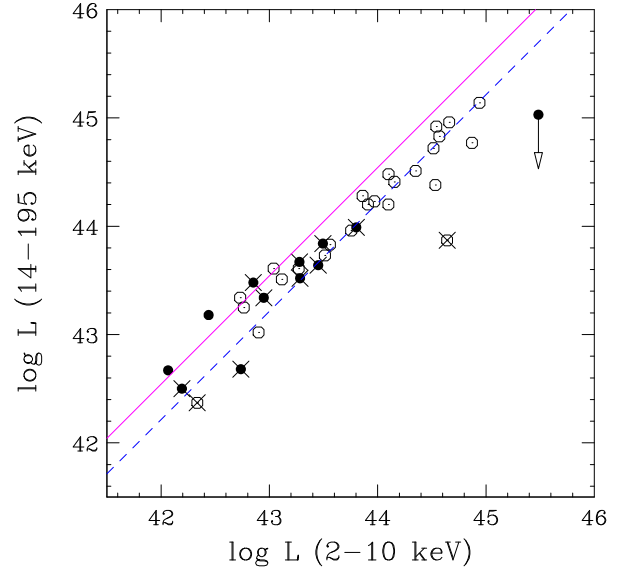


Fig. 5. Luminosity correlation between the 2–10 keV and 14–195 keV bands, determined from the MAXI/GSC and Swift/BAT surveys, respectively. No K-correction and that for absorption is applied to the 14–195 keV luminosity. The open and filled circles are X-ray unabsorbed ($\log N_H < 22$) and absorbed ($\log N_H \geq 22$) AGNs, respectively. Optical type 2 AGNs are marked with the diagonal crosses. The arrow denotes the upper limit for an AGN that is not detected in the Swift/BAT 58-month survey (Baumgartner et al. 2011). The dashed (blue) and solid (magenta) lines correspond to the ratio expected from a single power law spectrum with a photon index of 2.0 and 1.7, respectively.

et al. 2008). Because of the strong dependence of absorption fraction on the luminosity, we mostly detect only type 1 AGNs in the surveys at the high luminosity range, leading to the trend we see. Second possibility is the effect of a reflection component, which could be more significant at lower luminosities, as implied by the “X-ray Baldwin” effects (Iwasawa & Taniguchi 1993). The presence of a reflection hump in the spectra increases the observed flux in the hard X-ray band, peaked at ~ 20 keV, and hence the apparent slope over the 2–200 keV band becomes flatter. To distinguish these two effects, systematic studies of the broad X-ray band spectra of both type 1 and type 2 AGNs at various luminosity ranges are necessary.

5. Conclusion

We have constructed the local AGN X-ray luminosity function, utilizing our new sample consisting of 37 non-blazar AGNs at $z = 0.002\text{--}0.2$ detected in the 4–10 keV band from the first MAXI/GSC source catalog by Hiroi et al. (2011). The sample is highly complete $> 97\%$, and is less subject to uncertainties in the measured fluxes compared with the past all-sky survey missions above 2 keV. The conclusion of our work is summarized as follows.

- We strongly confirm the trend that there exist more absorbed AGNs at lower luminosities. The fraction of absorbed AGNs with $\log N_H = 22\text{--}24$ among

those with $\log N_{\text{H}} < 24$ corrected for the observational biases changes from 0.73 ± 0.25 at $\log L_{\text{X}} = 42\text{--}43.5$ to 0.12 ± 0.09 at $\log L_{\text{X}} = 43.5\text{--}45.5$. The estimated absorption distribution (N_{H} function) is consistent with the Swift/BAT and INTEGRAL results obtained above 10 keV.

- The shape of the intrinsic luminosity function of Compton thin AGNs can be fit with a smoothly connected double power law. For a fixed slope of $\gamma_1 = 0.84$ at a lower luminosity range, we obtain a break luminosity of $\log L_* = 43.3 \pm 0.4$ and a higher luminosity slope of $\gamma_2 = 2.0 \pm 0.2$. The L_* value is somewhat smaller than the HEAO-1 result. The integrated emissivity over $\log L_{\text{X}} = 41\text{--}47$ is found to be $(1.37 \pm 0.23) \times 10^{39} \text{ erg s}^{-1} \text{ Mpc}^{-3}$, which is only slightly larger than the previous estimate by HEAO-1. The space density agrees with the HEAO-1 result at $\log L_{\text{X}} \gtrsim 43.5$ but is larger at the lower luminosity range. This may be partially explained by the smaller biases against absorption in our survey in the 4–10 keV band, which lead to a better estimate of the N_{H} function.
- We compare our AGN luminosity function in the 2–10 keV band with those derived above 10 keV, by converting the luminosities by assuming a single power law spectrum. We find that the space densities matches with each other for $\Gamma \sim 1.7$ at $\log L_{\text{X}} < 44$, while they do for $\Gamma \sim 2.0$ at higher luminosities. This suggests the luminosity dependence of the averaged broad X-ray band spectra over the $\sim 2\text{--}200$ keV band. The trend is indeed confirmed by the luminosity correlation between the MAXI and Swift/BAT data in our sample.

The work is partially supported by the Ministry of Education, Culture, Sports, Science and Technology (MEXT), Grant-in-Aid No.19047001, 20041008, 20244015, 20540237, 21340043, 21740140, 22740120, 23000004, 23540265, and Global-COE from MEXT “The Next Generation of Physics, Spun from Universality and Emergence” and “Nanoscience and Quantum Physics”.

References

- Aird, J. et al. 2010, MNRAS, 401, 2531
 Barger, A. J. et al. 2005, AJ, 126, 632
 Baumgartner, W. H. et al. 2011, ApJS, submitted
 Beckmann, V., Gehrels, N., Shrader, C. R., & Soldi, S. 2006, ApJ, 638, 642
 Beckmann, V., Soldi, S., Shrader, C. R., Gehrels, N., & Produit, N. 2006, ApJ, 652, 126
 Burlon, D., Ajello, M., Greiner, J., Comastri, A., Merloni, A., Gehrels, N. 2011, ApJ, 728, 58
 Malizia, A., Bassani, L., Stephen, J. B., Di Cocco, G., Fiore, F., & Dean, A. J. 2003, ApJL, 589, L17
 Ebrero, J. et al. 2009, A&A, 493, 55
 Ferrarese, L., & Merritt, D. 2000, ApJL, 539, L9
 Gebhardt, K., et al. 2000, ApJL, 539, L13
 Gehrels, N. 1986, ApJ, 303, 336
 Gilli, R., Comastri, A., Hasinger, G. 2007, A&A, 463, 79
 Gültekin, K. et al. 2009, ApJ, 698, 198
 Häring, N. & Rix, H. 2004, ApJL, 604, L89
 Hasinger, G. 2008, A&A, 490, 905
 Hiroi, K., et al. 2011, PASJ, in press (arXiv:1108.5516)
 Hopkins, P. F., Hernquist, L., Cox, T. J., Robertson, B., Krause, E. 2007, ApJ, 669, 67
 Kormendy, J. & Bender, R. 2009, ApJL, 691, L142
 La Franca, F. et al. 2005, ApJ, 635, 864
 Magdziarz, P. & Zdziarski, A. A. 1995, MNRAS, 273, 837
 Magorrian, J., et al. 1998, AJ, 115, 2285
 Marconi, A. & Hunt, L. K. 2003, ApJL, 589, L21
 Matsuoka, M., et al. 2009, PASJ, 61, 999
 Mihara, T., et al. 2011, PASJ, in press (arXiv:1103.4224)
 Miyaji, T., Hasinger, G., & Schmidt, M. 2000, A&A, 353, 25
 Miyaji, T., Hasinger, G., & Schmidt, M. 2001, A&A, 369, 49
 Mould, J.R., et al. 2000, ApJ, 529, 786
 Piccinotti, G., Mushotzky, R. F., Boldt, E. A., Holt, S. S., Marshall, F. E., Serlemitsos, P. J., & Shafer, R. A. 1982, ApJ, 253, 485
 Revnivtsev, M., Sazonov, S., Jahoda, K., & Gilfanov, M. 2004, A&A, 418, 927
 Risaliti, G., Bianchi, S., Matt, G., Baldi, A., Elvis, M., Fabbiano, G., & Zezas, A. 2005, ApJL, 630, L129
 Sambruna, R. M. et al. 2011, ApJ, 734, 105
 Sazonov, S. & Revnivtsev, M. 2004, A&A, 423, 469
 Sazonov, S., Revnivtsev, M., Krivonos, R., Churazov, E., Sunyaev, R. 2007, A&A, 462, 57
 Shinozaki, K., Miyaji, T., Ishisaki, Y., Ueda, Y., & Ogasaka, Y. 2006, AJ, 131, 2843
 Silverman, J.D. et al. 2008, ApJ, 679, 118
 Sugizaki, M., et al. 2011, PASJ, in press (arXiv:1102.0891)
 Iwasawa, K. & Taniguchi, Y. 1993, ApJL, 413, L15
 Tueller, J., Mushotzky, R. F., Barthelmy, S., Cannizzo, J. K., Gehrels, N., Markwardt, C. B., Skinner, G. K., & Winter, L. M. 2008, ApJ, 681, 113
 Tueller, J., et al. 2010, ApJS, 186, 378
 Ueda, Y., Akiyama, M., Ohta, K., Miyaji, T. 2003, ApJ, 598, 886
 Winter, L. M., Mushotzky, R. F., Reynolds, C. S., & Tueller, J. 2009, ApJ, 690, 1322
 Winter, L. M. & Mushotzky, R. F. 2010, ApJ, 719, 737
 Yenko, B., Barger, A. J., Trouille, L., Winter, L. M. 2009, ApJ, 698, 380

Table 1. Source list of AGNs used in our study with spectral and luminosity information.

No.	MAXI Name	Counterpart	Type	Flux ^a	Redshift	Γ	N_{H}^b	$\text{Log } L_{\text{X}}^c$	Ref. ^d
3	MAXI J0048+320	Mrk 348	AGN2	2.42	0.0150	1.69	16	43.49	(1)
9	MAXI J0229+315	NGC 931	AGN1	1.77	0.0167	1.75	0.36	43.27	(1)
18	MAXI J0333-364	NGC 1365	AGN2	1.97	0.0055	2.11	29	42.74	(2)
24	MAXI J0423-569	1RXS J042601.6-571202	AGN1	1.71	0.1040	1.48	0	44.85	(1)
26	MAXI J0433+053	3C 120	AGN1	2.81	0.0330	2.00	0.05	44.10	(3)
29	MAXI J0510+166	IRAS 05078+1626	AGN1	2.77	0.0179	$2.07^{+0.55}_{-0.17}$	$0.0^{+1.9}$	43.56	(4)
31	MAXI J0516-001	Ark 120	AGN1	2.24	0.0323	1.90	0	43.97	(1)
40	MAXI J0552-075	NGC 2110	AGN2	8.13	0.0078	1.54	2.84	43.28	(1)
41	MAXI J0555+464	MCG +08-11-011	AGN1	3.66	0.0205	1.64	0.25	43.75	(1)
49	MAXI J0924-317	2MASX J09235371-3141305	AGN2	5.78	0.0423	$2.07^{+0.31}_{-0.17}$	$0.0^{+0.7}$	44.64	(4)
50	MAXI J0947-309	MCG -05-23-016	AGN2	6.58	0.0085	1.90	1.6	43.28	(1)
52	MAXI J1023+197	NGC 3227	AGN1	1.85	0.0039	1.52	6.6	42.06	(3)
56	MAXI J1105+725	NGC 3516	AGN1	1.84	0.0088	1.73	0.35	42.73	(1)
58	MAXI J1139-378	NGC 3783	AGN1	3.21	0.0097	1.60	0.09	43.04	(3)
61	MAXI J1144-184	2MASX J11454045-1827149	AGN1	1.87	0.0330	1.92	0	43.91	(1)
62	MAXI J1210+394	NGC 4151	AGN1	6.25	0.0033	1.65	3.4	42.44	(3)
67	MAXI J1240-052	NGC 4593	AGN1	1.96	0.0090	1.69	0	42.76	(3)
75	MAXI J1335-342	MCG -06-30-015	AGN1	3.42	0.0077	1.92	0.02	42.90	(3)
77	MAXI J1338+045	NGC 5252	AGN2	2.93	0.0230	1.55	4.34	43.80	(1)
80	MAXI J1349-302	IC 4329A	AGN1	7.44	0.0160	1.74	0.36	43.86	(3)
83	MAXI J1413-031	NGC 5506	AGN2	5.73	0.0062	1.72	3.23	42.95	(3)
84	MAXI J1418+251	NGC 5548	AGN1	3.06	0.0172	1.57	0	43.51	(3)
108	MAXI J1716-629	NGC 6300	AGN2	1.65	0.0037	1.83	21.5	42.19	(1)
109	MAXI J1741+185	4C +18.51	AGN1	1.66	0.1860	$1.90^{+0.17}_{-0.00}$	$4.0^{+8.3}_{-4.0}$	45.47	(4)
115	MAXI J1835+328	3C 382	AGN1	2.69	0.0579	1.86	0.06	44.56	(5)
117	MAXI J1837-653	ESO 103-035	AGN2	2.26	0.0133	1.96	20.3	43.45	(3)
118	MAXI J1839+798	3C 390.3	AGN1	2.85	0.0561	1.64	0.03	44.53	(3)
119	MAXI J1851-783	2MASX J18470283-7831494	AGN1	1.45	0.0741	1.93	0.01	44.53	(3)
122	MAXI J1920-586	ESO 141-G055	AGN1	2.52	0.0360	1.72	0	44.09	(3)
127	MAXI J2009-611	NGC 6860	AGN1	1.61	0.0149	1.64	0.10	43.11	(6)
129	MAXI J2041+750	4C +74.26	AGN1	1.83	0.1040	1.86	0.18	44.93	(1)
130	MAXI J2044-107	Mrk 509	AGN1	3.32	0.0344	1.49	0	44.15	(3)
132	MAXI J2135-626	1RXS J213623.1-622400	AGN1	1.48	0.0588	$2.10^{+0.87}_{-0.20}$	$0.0^{+3.9}$	44.35	(4)
135	MAXI J2202-319	NGC 7172	AGN2	2.02	0.0087	1.69	8.2	42.85	(3)
138	MAXI J2235-259	NGC 7314	AGN2	2.46	0.0048	1.85	0.72	42.33	(3)
140	MAXI J2253-177	MR 2251-178	AGN1	2.98	0.0640	1.41	0.28	44.64	(1)
142	MAXI J2305-085	Mrk 926	AGN1	3.92	0.0469	1.61	0	44.51	(3)

^a: observed flux in the 4–10 keV band in units of $\text{erg cm}^{-2} \text{s}^{-1}$ ^b: intrinsic luminosity (before absorption) in the 2–10 keV band in units of erg s^{-1} ^c: in units of 10^{22} cm^{-2} ^d: reference for the X-ray spectra: (1) Winter et al. (2009), (2) Risaliti et al. (2005), (3) Shinozaki et al. (2006), (4) MAXI/GSC hardness ratio (this work), (5) Sambruna et al. (2011), (6) Winter & Mushotzky (2010)**Table 2.** Best fit parameters of the N_{H} function and 2–10 keV luminosity function of AGNs in the local universe.

N_{H} function			2–10 keV Luminosity Function			
ϵ	Ψ_{44}	β	A^a	γ_1	γ_2	L_*^b
1.3 (fixed)	0.37 ± 0.03	0.23 ± 0.02	$(1.49 \pm 0.25) \times 10^{-5}$	1.00(fixed)	$2.13^{+0.28}_{-0.21}$	$43.59^{+0.33}_{-0.41}$
			$(4.2 \pm 0.7) \times 10^{-5}$	0.84(fixed)	$2.03^{+0.21}_{-0.17}$	$43.30^{+0.31}_{-0.38}$
			$(8.8 \pm 1.5) \times 10^{-5}$	0.62(fixed)	$1.95^{+0.17}_{-0.14}$	$43.03^{+0.28}_{-0.33}$

^a: in units of $[h_{70}^3 \text{ Mpc}^{-3}]$ ^b: in units of $[h_{70}^{-2} \text{ erg s}^{-1}]$ The error is 1σ for a single parameter.